AD-A083 344 LOCKHEED MISSILES AND SPACE CO INC PALO ALTO CA PALO --ETC F/G 7/5
TIME- AND ENERGY-DEPENDENT EFFECTS IN CRYSTAL SPECTROMETERS.(U)
NOV 78 D A KOHLER, J G PRONKO, R K BARDIN DNA001-78-C-0124
UNCLASSIFIED LMSC/D634919 DNA-4774F NL

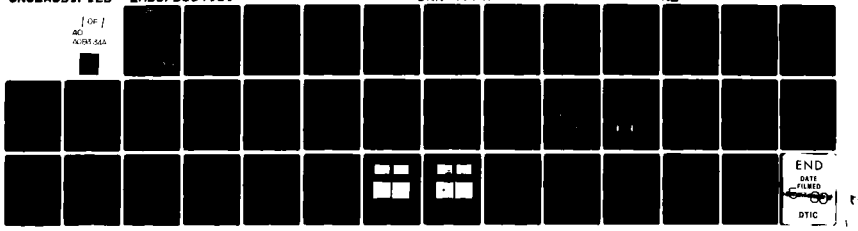

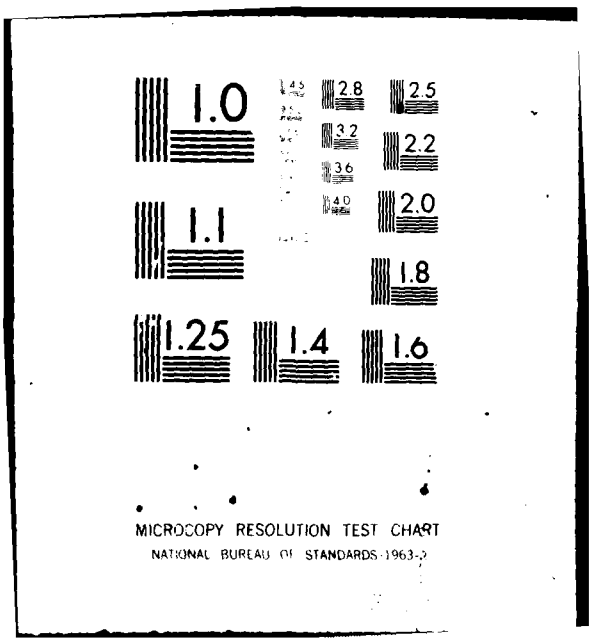
1.0
2.8
2.5
3.2
2.2
3.6
4.0
2.0
1.1
1.8
1.25
1.4
1.6
MICROCOPY RESOLUTION TEST CHART
NATIONAL BUREAU OF STANDARDS-1963-A

(12) LEVEL III

NW

DNA 4774F

TIME- AND ENERGY-DEPENDENT EFFECTS IN CRYSTAL SPECTROMETERS

Lockheed Palo Alto Research Laboratory
3251 Hanover Street
Palo Alto, California 94304

30 November 1978

Final Report for Period 1 February 1978—30 November 1978

CONTRACT No. DNA 001-78-C-0124

THIS WORK SPONSORED BY THE DEFENSE NUCLEAR AGENCY
UNDER RDT&E RMSS CODE B345078462 J11AAXA01303 H2590D.

Prepared for
Director
DEFENSE NUCLEAR AGENCY
Washington, D. C. 20305

Destroy this report when it is no longer needed. Do not return to sender.

PLEASE NOTIFY THE DEFENSE NUCLEAR AGENCY, ATTN: STTI, WASHINGTON, D.C. 20305, IF YOUR ADDRESS IS INCORRECT, IF YOU WISH TO BE DELETED FROM THE DISTRIBUTION LIST, OR IF THE ADDRESSEE IS NO LONGER EMPLOYED BY YOUR ORGANIZATION.

UNCLASSIFIED

SECURITY CLASSIFICATION OF THIS PAGE *(When Data Entered)*

REPORT DOCUMENTATION PAGE	READ INSTRUCTIONS BEFORE COMPLETING FORM
1. REPORT NUMBER: DNA 4774F	2. GOVT ACCESSION NO.: AD-A083 347
3. RECIPIENT'S CATALOG NUMBER:	
4. TITLE *(and Subtitle)*: TIME- AND ENERGY-DEPENDENT EFFECTS IN CRYSTAL SPECTROMETERS	5. TYPE OF REPORT & PERIOD COVERED: Final Report for Period 1 Feb 78—30 Nov 78
	6. PERFORMING ORG. REPORT NUMBER: LMSC/D634919
7. AUTHOR(s): D. A. Kohler, R. K. Bardin, J. G. Pronko, L. F. Chase	8. CONTRACT OR GRANT NUMBER(s): DNA 001-78-C-0124 new
9. PERFORMING ORGANIZATION NAME AND ADDRESS: Lockheed Palo Alto Research Laboratory, 3251 Hanover Street, Palo Alto, California 94304	10. PROGRAM ELEMENT, PROJECT, TASK AREA & WORK UNIT NUMBERS: Subtask J11AAXAX013-03
11. CONTROLLING OFFICE NAME AND ADDRESS: Director, Defense Nuclear Agency, Washington, D.C. 20305	12. REPORT DATE: 30 November 1978
	13. NUMBER OF PAGES: 38
14. MONITORING AGENCY NAME & ADDRESS *(if different from Controlling Office)*	15. SECURITY CLASS *(of this report)*: UNCLASSIFIED
	15a. DECLASSIFICATION/DOWNGRADING SCHEDULE

16. DISTRIBUTION STATEMENT *(of this Report)*

Approved for public release; distribution unlimited.

17. DISTRIBUTION STATEMENT *(of the abstract entered in Block 20, if different from Report)*

18. SUPPLEMENTARY NOTES

This work sponsored by the Defense Nuclear Agency under RDT&E RMSS Code B345078402 J11AAXAX01303 H2590D.

19. KEY WORDS *(Continue on reverse side if necessary and identify by block number)*

X-Ray Damage in Crystals
Crystal Spectrometers
Crystal Spectrometer Damage
Crystal Spectrometer X-Ray Dose Limits
Dose Limits for Crystal Spectrometers

20. ABSTRACT *(Continue on reverse side if necessary and identify by block number)*

The behavior of the organic crystal diffraction element KAP under intense pulsed x-ray irradiation has been studied using the Lockheed Palo Alto Research Laboratory (LPARL) high-power Nd-glass pulsed-laser facility. The distortions in spectral data which result from high dose-rate irradiation have been elucidated. The x-ray heating-induced crystal expansion has been observed and shown to imply heating of the crystal to far beyond its normal melting point while maintaining high Bragg reflection efficiency. Streak

DD FORM 1 JAN 73 1473 EDITION OF 1 NOV 65 IS OBSOLETE

UNCLASSIFIED

SECURITY CLASSIFICATION OF THIS PAGE *(When Data Entered)*

20. ABSTRACT (Continued)

camera-studies of the phenomena provide further detail and show that the total Bragg reflection efficiency can remain high even for the several ns duration of the x-ray heating pulse.

PREFACE

This final report is submitted to the Defense Nuclear Agency by the Lockheed Palo Alto Research Laboratory for contractual research performed under Contract DNA001-78-C-0124 for the period February 1978 through November 1978.

TABLE OF CONTENTS

LIST OF ILLUSTRATIONS

Section 1
INTRODUCTION

Crystal and mirror spectrometers have become standard items in detection systems which are used to produce spectral information on intense x-ray sources, such as are used in underground weapons effects tests. However, there has always been some concern about the effects of the relatively large amount of x-ray energy deposited in the dispersive element during some of these measurements. This concern is centered on possible changes in the diffractive and/or reflective properties of the spectrometer dispersive element. For instance, there have been in some cases, indications of lattice parameter changes due to the substantial x-ray energy deposited in the surface of the crystal diffraction element of a crystal spectrometer.

This report describes the results of the first laboratory program, the objective of which was to experimentally determine the nature and extent of such changes in spectrometer dispersive elements when subjected to high input energy and a correspondingly high temperature rise. The specific area studied in this program was the behavior of an x-ray diffractive crystal when subjected to such high energy input. An intense low-energy x-ray irradiation produced by a high-power Nd-glass laser has proved adequate to heat the crystal sample surface regions to the high temperatures required for this study. This approach proves ideal since the heating method is, of course, the same as involved in the field tests which were originally of concern. The technique makes it possible to heat a diffractive crystal to very high temperatures with resultant expansion of the crystal lattice spacing of as much as several percent. The corresponding effects upon spectrometer performances have been determined--preeminent among them being a very substantial loss of spectral resolution with the line always being broadened asymmetrically with a long tail on the high-energy side of the normal line. Detailed discussion of these and other effects will be found in Sections 4 and 5, following.

A general overview of the LPARL high-power Nd-glass laser used in these studies and the x-ray production techniques using this laser are presented in Section 3. The experimentally-observed behavior of the spectral lines under these conditions with passive (time-integrated) film recording is discussed in Section 4 together with what one can infer as to the nature of the phenomena. Section 5 discusses the studies made with a streak camera of the time-dependent behavior of the Bragg-reflection efficiency of the crystal under intense irradiation. Finally, in Section 6 a summary of results and conclusions is presented together with recommendations for possible improvements and extensions of these measurements.

Section 2
GENERAL CONSIDERATIONS

The principal effect expected for high dose-rate x-ray irradiation of a crystal is thermal expansion of the lattice due to the resultant temperature rise. The corresponding effect in its use in a crystal spectrometer is then a change in Bragg angle of the order of the crystal linear expansion coefficient times the temperature rise. It was expected, before the work described in this report was undertaken, that temperature rises up to the crystal melting point and/or decomposition temperatures were the appropriate values to be used in estimating possible magnitudes of the effect. Allowing perhaps 100 to 200 K for a reasonable temperature rise to melting or decomposition for an organic crystal and a typical expansion coefficient of a few times $10^{-5}K^{-1}$, one might expect fractional line shifts of the order of a few times 10^{-3}. Such values for line shifts of rather less than one percent are not much worse than the actual resolutions typically used in field experiments. For many purposes, accordingly, the loss of resolution due to such thermal expansion shifts, although experimentally visible, would be quite tolerable. Of course, higher melting point crystals such as the LiF often used in such applications might show correspondingly larger shifts. With the general background as presented above, one can now proceed to the problem of defining practical approaches to the experimental study of such effects.

From the point of view of defining the requirements for a practical experimental measurement of thermally-induced crystal spectrometer errors, it is clearly desirable to be able to heat at least selected crystals to their melting points in times of the order of a few nanoseconds. This heating should take place over a volume covering at least a substantial fraction of the diffraction depth of the crystal ($\sim$ 1 μm). Observation of the crystal diffraction efficiency as a function of energy deposition

should be made with a time resolution that is narrow compared to the heating time. Ideally the experiment design should also incorporate a system calibration which could be used simultaneously with the primary measurement.

The heating requirement is a major restriction on experiment design. One obvious candidate technique is pulsed-laser optical heating using the LPARL high-power pulsed Nd-glass laser facility. Ample power is available for heating on time scales down to the subnanosecond level. Because of the depth of heating requirement, however, the technique is restricted to crystals and mirrors with a rather narrow range of optical absorption coefficients at the laser wavelength. For crystals, it would probably be necessary to manufacture them with an in situ dye, either by diffusion of an appropriate dye or by crystal growth from a dye-bearing solution, in order to meet the absorption requirement. Radiation-induced color centers might also provide suitable absorption levels. Opaque crystals would not be usable as surface heat would take too long to conduct into the active region.

Other sources of penetrating radiation available at LPARL include a Febetron 706, DC x-ray machines, and a Van de Graaff proton accelerator. However, none of these are capable of the required power deposition density.

The most attractive candidate technique is direct x-ray heating using x rays produced from plasmas generated by the LPARL laser facility. This provides a good match of heating depth to penetration depth in any crystal although, for intensity reasons, it is restricted to photon energies less than about 2.0 keV. The available x-ray yield is sufficient to heat typical crystal surfaces to approximately 200 K above ambient using the copper L lines at distances of about 2.5 mm from the target. Higher temperatures or larger distances may be attained using copper radiation in the 200 to 400 eV range. Pulse widths of 2 to 10 ns and even greater are readily available.

It was clearly desirable to measure the crystal diffraction efficiencies using a source of x-ray line radiation of sufficient intensity to permit time- and energy-resolved measurements of the reflected intensities. Because of the time scale of the heating, it was necessary to use pulsed x-ray line sources and again the only reasonable candidate was the LPARL laser facility.

Even with this x-ray source, the detection system must be fairly sensitive. The best combination of sensitivity and time resolution presently available is provided by a NE111 high-speed scintillator coupled to a streak camera. Our estimates indicated that this system should provide adequate sensitivity at the time resolution permitted by the scintillator pulse FWHM, which is of the order of 0.6 ns, quite sufficient for the 6-10 ns duration heating pulses to be used. In addition, the spatial resolution of the streak camera provides the desired energy resolution.

From the above considerations, it was decided that the only practical approach was to carry out the experiments with the LPARL laser facility in which spectrometers using dispersive elements were sufficiently close-coupled so as to cause local x-ray heating of the dispersive element. A suitable line or lines from the heating spectrum itself would be chosen both for passive recording on x-ray film and for use with the streak camera/scintillator combination.

The direct optical heating alternative described above would not be explored unless it was required to increase the heating rate or to change the timing of the heating relative to the x-ray probe. It is noted in this regard that the optical heating technique presents an additional calibration problem in determining the heating energy deposition density. For x-ray heating, of course, the energy deposition is readily calculable from the measured incident-power spectral distribution and known absorption cross-sections.

The experimental objective then, was to cover the study of the diffractive behavior of a suitable crystal within the x-ray power limitation of the laser x-ray source, at power densities up through those causing surface melting or spall. Accordingly, in the following section, a description of the pulsed laser-produced x-ray facility is presented.

Section 3
LPARL LASER-PRODUCED X-RAY FACILITY

3.1 PULSED-LASER SYSTEM

The LPARL pulsed-laser system has been designed for maximum versatility when employed as a pulsed x-ray source. The choice of Nd-glass as the laser medium provides the shortest pulses that can be generated by current laser technology. These pulses can be stretched and/or stacked to provide, in principle, arbitrary pulse shapes and lengths up to 30 ns or greater. Good beam quality is maintained so that 75 percent of the total laser output can be focused into an 80-μm diameter target spot. For instance, for a 10-J, 6-ns pulse this implies a power density of $6 \times 10^{13} W/cm^2$ at the focal spot, quite adequate for efficient x-ray production from targets having a wide range in Z. The choice of target Z together with the use of appropriate filters, makes it possible to tailor the x-ray spectrum to meet the needs of a particular experiment. The target chamber is designed to make possible the rapid positioning or interchange of various targets and filters and the simultaneous use of several different types of x-ray detectors.

A schematic diagram of the LPARL laser facility is shown in Fig. 1. The oscillator is normally operated in a mode-locked (saturable dye) configuration that operates at a wavelength of 1.06 μm. The output of the oscillator then consists of a train of pulses 7 ns apart, and each pulse has a width at half-maximum of approximately 15 ps. The width of the pulses can be varied up to 1 ns by the insertion of appropriate etalons into the cavity. However, pulses of still greater width are available instead by Q-switching the oscillator cavity (the so-called "giant pulse mode"), and various pulse shapes can then be generated, in principle, by employing stacking techniques. The selection of a single pulse from the mode-locked train or segment from the giant pulse is accomplished by an optical switch consisting of a

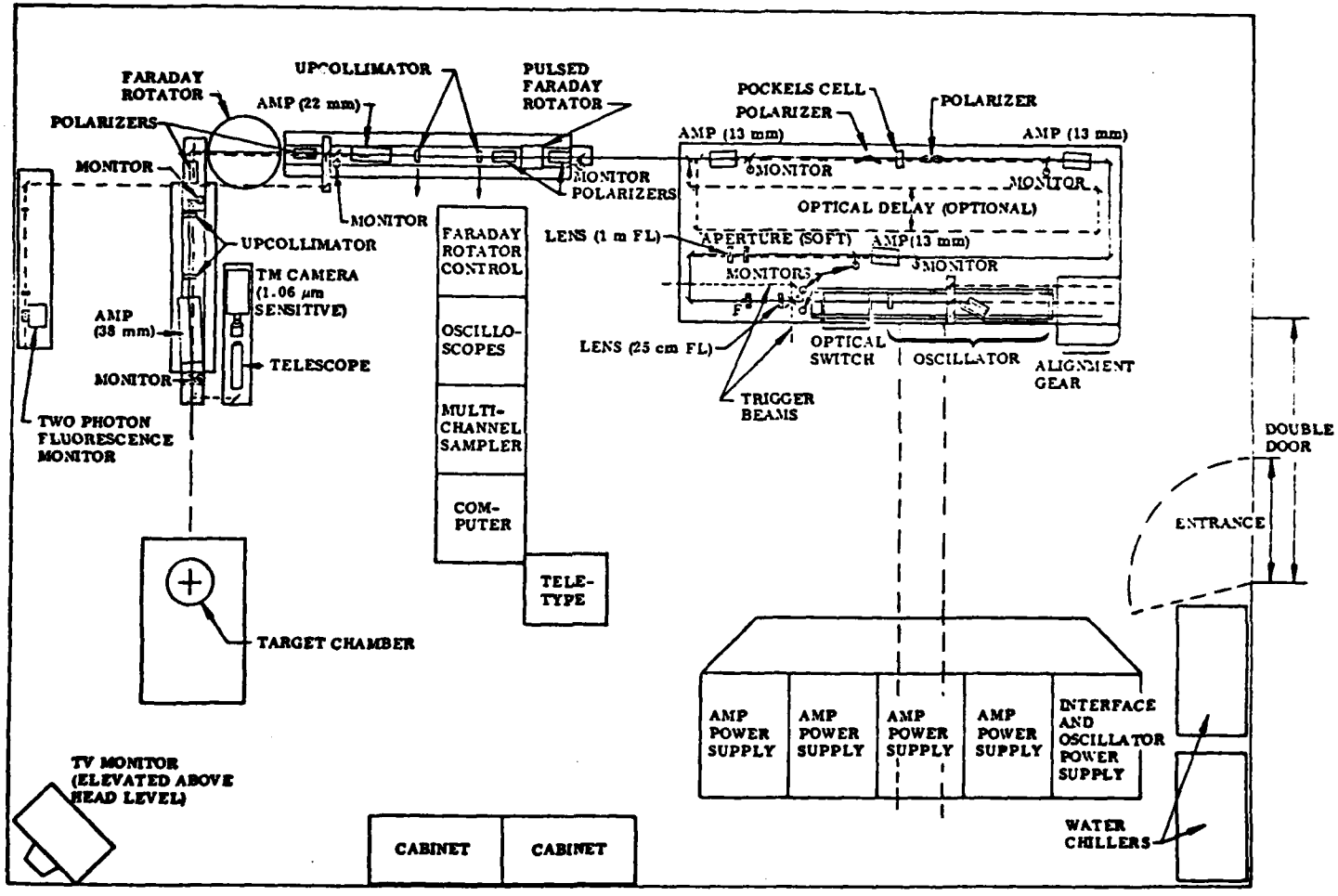

Figure 1

The LPARL High-Power Pulsed-Laser Facility

Pockels cell between two crossed polarizers. A second similar switch between the second and third amplifiers provides additional beam cleanup and isolation against the beam reflected from the target.

The beam, which is approximately 3 mm in diameter at the exit of the optical switchout system, passes through a 2:1 upcollimating system consisting of two positive lenses with a pinhole spatial filter positioned at the crossover point. This produces a beam diameter of 6 mm at the entrance of the first Nd-glass amplifier, and the beam is diverged slightly so that its diameter is about 12 mm when it emerges from the third amplifier. The beam energy at this point is in the range 250 to 500 mJ for a 200-ps pulse. All components of the laser system to this point are mounted on a 1.22-m by 3.05-m granite table with a folded optical path, as illustrated in Fig. 1. A fourth amplifier stage boosts the energy into the 1- to 2-J range. The fifth and final amplifier stage is 38 mm in diameter and can bring the beam energy up to $\sim$ 10 J for a 200-ps pulse and somewhat greater for pulses of several ns duration. This amplifier is preceded by a 1.7:1 upcollimator, which increases the beam diameter to about 3.0-3.5 cm.

In order to prevent damage to system components by the beam which is reflected from the target and subsequently amplified, a number of isolation elements have been installed. One of these, already mentioned, is the pinhole aperture positioned just after the switch-out system. This aperture trims high-order transverse spatial modes in both the incident and return beam, and thus provides the double function of beam cleanup and isolation. The two Pockels cells also serve as isolation elements, since they function as optical gates which close in time to block any reflected return. The principal isolation element is the pulsed Faraday rotator system which yields a forward/backward transmission ratio of the order of 1000:1 and is placed just before the fourth amplifier.

3.2 TARGET CHAMBER FOR X-RAY PRODUCTION

The laser beam from the 38-mm diameter amplifier is then directed to the target chamber where it is focused by an aspheric lens of 117-mm focal length to a small spot ~ 50-100 μm in diameter on a target at the chamber center. The target chamber which was used to hold the laser target and crystal to be irradiated is cylindrical in shape, measuring 30.5 cm in diameter by 20.3 cm deep, with a removable cover. The target holder is mounted on a 3-axis table which, through controls external to the chamber, provides three translational degrees of freedom for positioning the target, as well as a rotation about the vertical axis. These degrees of freedom enable any desired target spot to be brought into spatial coincidence with the focal point of the beam. The chamber is evacuated to approximately 5×10^{-6} torr by a standard 10-cm oil diffusion pump backed by a mechanical roughing pump. The design of the chamber readily accommodates a full range of plasma diagnostic experiments, and can be interfaced with a curved-crystal x-ray spectrometer, various calorimeters, a fast x-ray diode, an ion spectrometer, and an assortment of scintillator-photodiode detectors. Much of this diagnostic instrumentation was developed under previous DNA contracts.

3.3 X-RAY PRODUCTION

The total x-ray energy production efficiency can, depending on the target and the power level used, range from a small fraction of one percent of the input laser beam energy to several percent. The total x-ray energy yield for a typical laser pulse is very difficult to measure accurately with calorimeters but several mJ/sr in the keV energy region is indicated while several times that in the low-energy range of perhaps 200 to 600 eV has been observed. For instance, earlier measurements for a 2.7-J shot with a 200-ps pulse length have yielded ~ 125 mJ/4 πsr of line radiation at ~ 1-keV energy and above. At the same time ~ .25 J/4 πsr was observed in the two regions ~ 150 - 300 eV and ~ 650 -11000 eV jointly where the gap from

300 to 650 eV resulted from a necessary filter. Thus the total radiation in this lower energy region presumably is substantially higher than the 0.25 J/4 πsr recorded. For the longer pulses of interest in this work, the laser power density is substantially reduced and hence the efficiency of x-ray energy production will be reduced. However, considering the 8-15-J energy in the longer pulses, it is reasonable to assume that the x-ray yield in the range well below 1 keV would be at least several mJ/sr for the typical observations described in Section 4.

Section 4
TIME-INTEGRATED EFFECTS IN CRYSTAL SPECTROMETER ELEMENTS

4.1 INTRODUCTION

In this phase of the work, the basic phenomena of the distortion of spectrometer data by intense x-ray beams were explored. It was necessary, of course, to determine what level of distortion could be produced in a typical crystal diffraction spectrum by the LPARL laser-generated x-ray source. This in turn, would define the experimental sensitivity needed for effective study of the detailed nature of the distortion and its mode of generation. With the heating source available, it was found that very large spectral distortions could be produced so that a rather small crystal spectrometer proved sufficient to effectively study the relevant phenomena.

4.2 EXPERIMENTAL STUDY OF SPECTRAL DISTORTIONS IN A CRYSTAL SPECTROMETER

For this work, x-ray pulses of about 6-7-ns duration were used. These were produced with the LPARL Nd-glass laser reconfigured from its normal mode-locked arrangement to that of a giant pulse Q-switched system. Pulses of about 7-ns width were then switched out of the giant pulse with an appropriate Pockels cell-polarizer optical gate. The resulting pulses, after amplification to the 7-15-J level, were then focused onto a planar copper target at an angle of incidence of about 40°. The resulting x rays were reflected from the crystal under study onto a small strip of type RAR x-ray sensitive film protected by a 2.5×10^{-3}-cm thick beryllium foil. This was all placed within the evacuated target chamber about 11 cm from the target and at 90° to the laser beam direction. (See Fig. 2 for a schematic representation of this experimental arrangement.)

The crystal diffraction element studied was a thin, flat cleaved piece of KAP (potassium acid phthalate) mounted on a glass slide. This

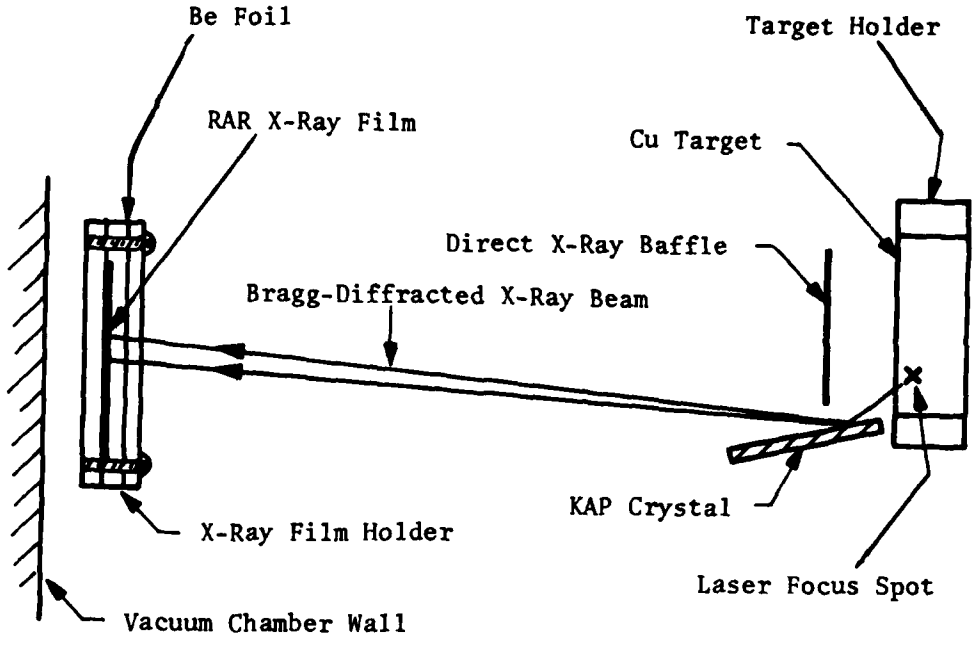

Figure 2

Schematic of the Experimental Arrangement
for the Crystal Spectrometer Time-Integrated Studies

A vertical section is shown through the target point and the film holder mid-plane. The x-ray point source at the laser focus is ~ 1 cm from the crystal at the point where the 980 eV-copper doublet is Bragg reflected. A 2.5 x 10^{-3}-cm thick Be foil is interposed between the target and crystal when a low-intensity or "calibration" shot is required.

assembly was mounted on a mechanical support which allowed the crystal to be placed as close as a few millimeters from the x-ray source. The reflection angle was set at about 28^{o} in order to survey the 1-keV region of the copper x-ray spectrum. Two different experimental configurations were used jointly to investigate any x-ray reflection anomalies. First, a spectrum was taken with a 2.5×10^{-3}-cm thick Be foil interposed between the x-ray source and the KAP crystal. This resulted in a spectrum showing the strong doublet at about 980 eV and a number of lines in the 1.1-1.3 keV range. This spectrum which was taken at low dose levels because of the attenuation of the x rays by the Be foil, represents the performance of the crystal under largely undisturbed conditions, i.e., a "calibration" spectrum. The Be foil was then removed and another shot was taken--all other conditions remaining the same. The resulting spectrum displays drastic differences from the low dose-rate spectrum. (See inserts in Fig. 3 and Fig. 4 for reproductions of typical spectra taken at a 1-cm source-to-crystal separation.) The calibration spectra always show relatively symmetric and narrow lines. The high dose-rate spectra, on the other hand, show lines with a sharp edge at the high Bragg-angle side and a strongly-broadened or smeared structure on the low-angle or high-energy side. This effect corresponds to an increased crystal lattice spacing or expansion of the solid. It was also found that successive shots at the same place on the crystal with and without a Be filter always exhibited this characteristic difference i.e., the crystal either healed itself after each shot or the strongly-disturbed surface layer was spalled away leaving normal material ready for the next shot. Densitometer traces have been made of these spectra and typical results are displayed in Figs. 3 and 4 for the low dose-rate and high dose-rate irradiations, respectively.

The x-ray induced crystal expansion indicated by these data ranges up to the order of several percent (in linear expansion) and shows that extremely large crystal expansions can be generated without significant destruction of the Bragg reflection. In fact, these expansions appeared to be large enough to indicate that even the melting point (or other dissolution phase change) was probably exceeded while still preserving

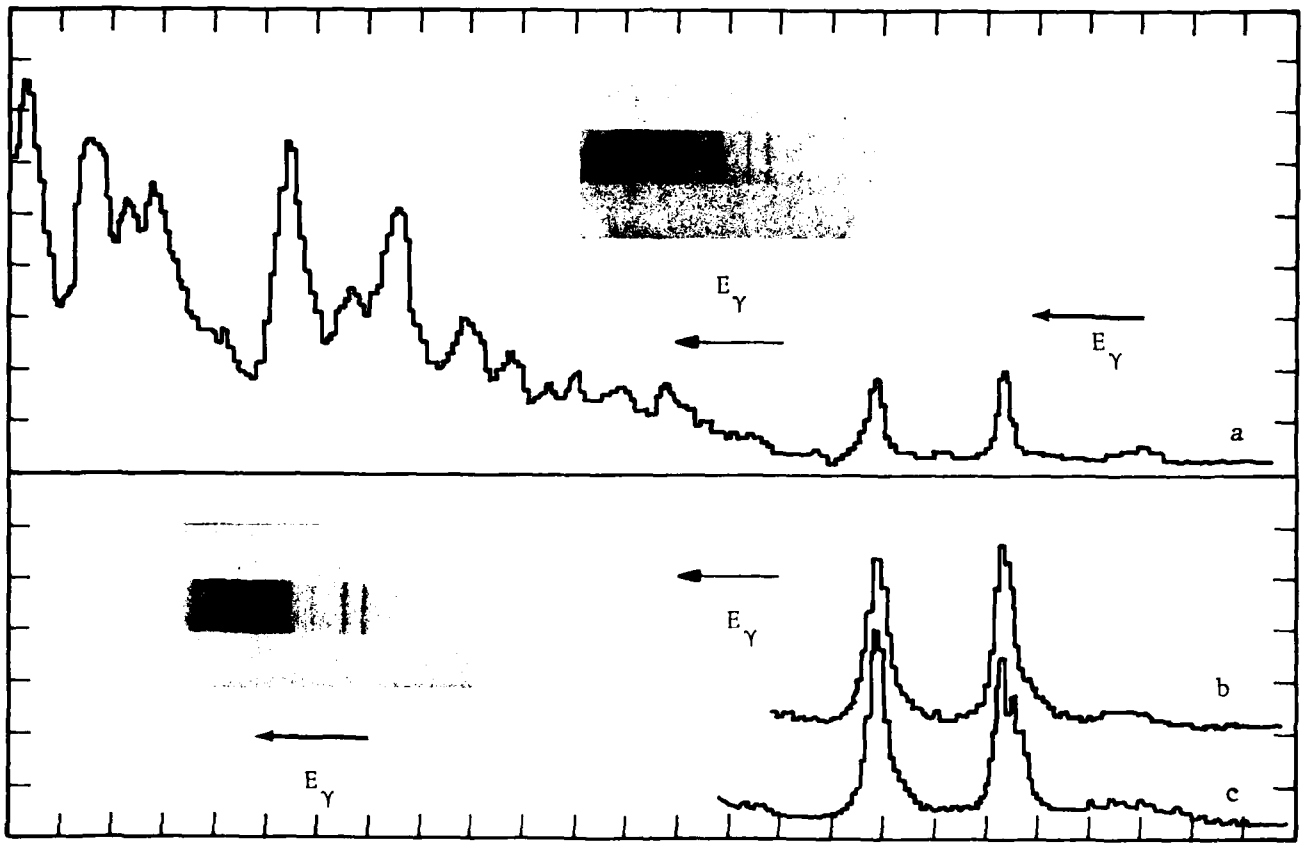

FIGURE 3 Low X-Ray Dose-Rate Spectra Taken With a KAP Crystal Spectrograph

Shown are enlargements (x 2.5) of two typical crystal diffraction x-ray spectra from a laser irradiated copper target (the two inserts). These were taken with a 2.5 x 10^{-3}-cm thick Be foil interposed between the x-ray source and the KAP crystal. The separation between the x-ray source and the crystal reflection zone was ~ 1 cm. The isolated doublet at the right end is the 980-eV Cu doublet. The curves are densitometer traces of these spectrograms. Curve a is a densitometer trace across the spectrogram in the upper insert and curves b and c are traces at different positions for the spectrogram in the lower insert.

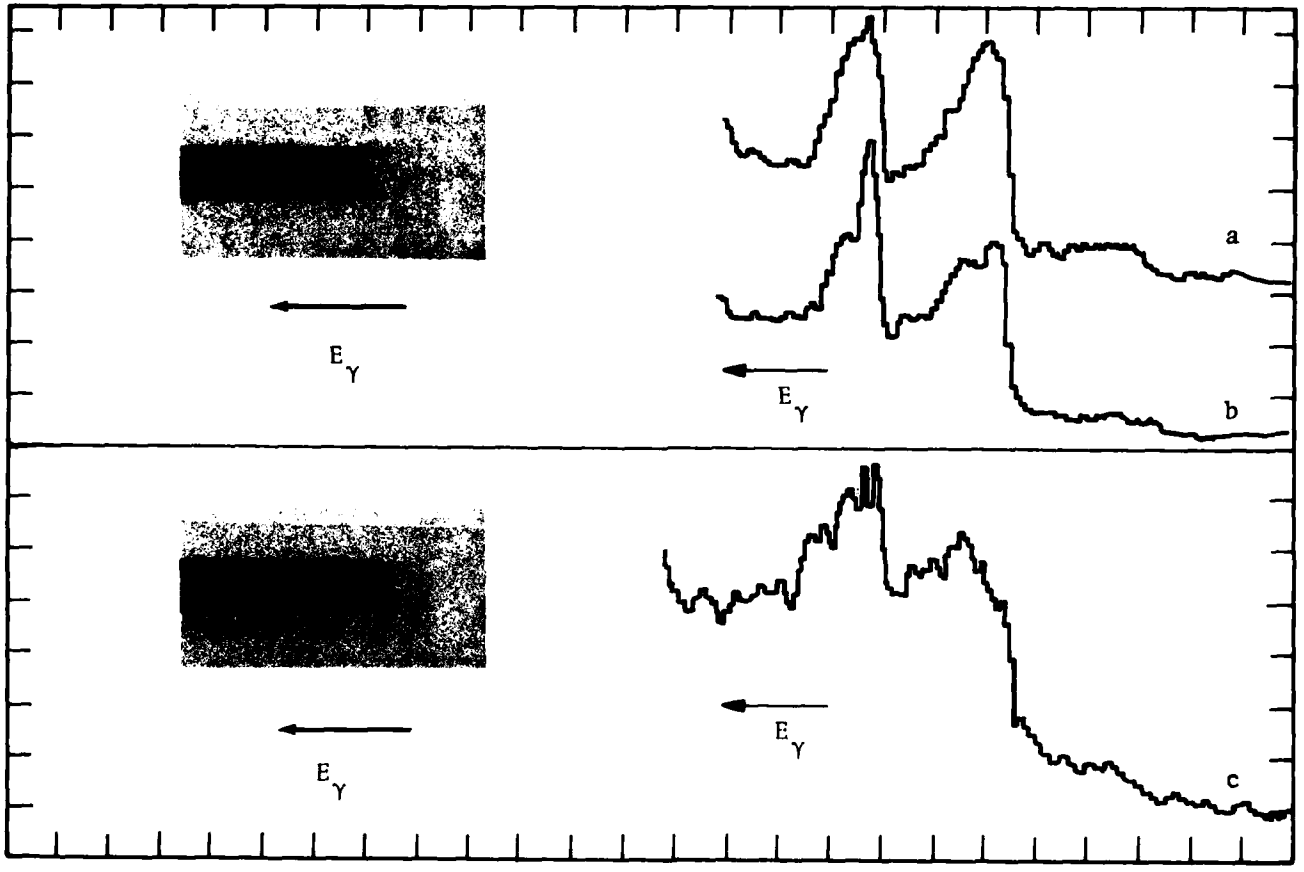

FIGURE 4 High X-Ray Dose-Rate Spectra Taken With a KAP Crystal Spectrograph

Shown are enlargements (x 2.5) of two typical crystal diffraction x-ray spectra from a laser irradiated copper target (the two inserts). These were taken without the Be filter interposed between the x-ray source and the KAP Bragg scattering crystal. These spectra were taken with the same 1-cm target-to-crystal separation as for those shown in Figure 3. The isolated but very distorted 980 eV Cu doublet is still evident at the right in these spectrograms. Curves a and b are traces at two different positions on the spectrogram shown in the upper insert. Curve c is a similar trace for the spectrogram in the lower insert and shows an extreme broadening corresponding to a linear crystal expansion substantially greater than 4%.

the crystal lattice. If the latter is correct, then it follows that a superheated crystalline solid phase was created in these experiments.

4.3 MELTING POINT AND THERMAL EXPANSION COEFFICIENT OF KAP CRYSTAL

In order to more completely assess the significance of the observed crystal expansions as described in the above sub-section, knowledge of certain thermal properties of the KAP crystal is needed. In particular, the thermal expansion coefficient is necessary in order to infer from the expansion the corresponding temperature rise. In addition, the melting and/or decomposition temperature is needed to evaluate the extent of crystal super heating, if any.

First a literature search produced the result of $4.0 \pm .2 \times 10^{-5} K^{-1}$ for the KAP room-temperature thermal expansion coefficient. This result, if e.g., assumed to be temperature independent, together with the observed expansions would correspond to a temperature rise of $\sim$1000 to 2000 K. Further work was done in the LPARL laboratory to establish the melting and/or decomposition temperature for KAP. Simple visual examination of a progressively heated piece of KAP crystal indicated an apparent melting and onset of gas evolution at about 300°C with however poor definition of the real onset temperature. A standard thermogravimetric analysis (weight change vs. temperature) for KAP was then carried out over the temperature interval 300 to 780 K at 40 K/min. The principal feature observed in this data was a 40% weight loss with an onset at about 540 K or 267°C and a steep increase in loss rate starting at about 555 K or 282°C.

Finally the temperature dependence of the thermal expansion coefficient was directly measured in the LPARL laboratory. X-ray diffraction measurements were made to determine the expansion coefficient for KAP over the temperature range of 20°C to 225°C. The specimen was heated in a temperature-controlled and monitored hot stage attached to a Norelco diffractometer. A calibrated Cr-Al thermocouple was used to monitor the temperature of the hot stage. Scans using CuK_{α} irradiation were made

at a number of temperatures over the quoted range. The highest temperature scan indicated the possibility of some phase transformation (melting?). The resulting data are shown in Fig. 5 in the form of a graph of the change in lattice spacing, Δd, divided by the room temperature lattice spacing, d_0, vs. temperature. Within errors the temperature dependence of the lattice spacing is completely linear showing that over this temperature interval the expansion coefficient is in fact constant. The value for the expansion coefficient resulting is $4.6 \pm .3 \times 10^{-5} K^{-1}$, in adequate agreement with the above quoted room temperature value--a combined average of $4.2 \pm .3 \times 10^{-5} K^{-1}$ is then a reasonable value to assume for this latter quantity.

4.4 X-RAY INDUCED TEMPERATURE RISE FOR KAP

The expansion data discussed in 4.1 and 4.2, together with the thermal data discussed in 4.3 suggest that temperature increases of as much as 1000 to 2000 K have been produced with the material still remaining crystalline. This follows if one is willing to use the measured expansion coefficient for the full expansion range observed. It should be noted that up to about 225°C no deviation from linearity was found. This result excludes any anomalous increase in expansion coefficient (as the melting point is approached) which could have accomodated the very large expansions observed without a correspondingly large temperature rise. (To postulate a change above this temperature to a new crystalline form with different lattice spacing also seems very unlikely since if the initial crystalline bonds are broken it would presumably be very difficult to solidify to a new form on such a short time scale, especially when the temperature is evidently still being increased.) Thus the above result lends further strength to the suggestion made previously that the KAP has been superheated to very high temperatures (as much as 1000 K to 2000 K above room temperature) without destruction of the Bragg reflection efficiency. The melting and/or decomposition, which normally begins at or slightly above this temperature, apparently does not have sufficient time to take place during the few ns involved as shown by the nature of the spectrograms themselves. Since the crystal does remain intact, it is

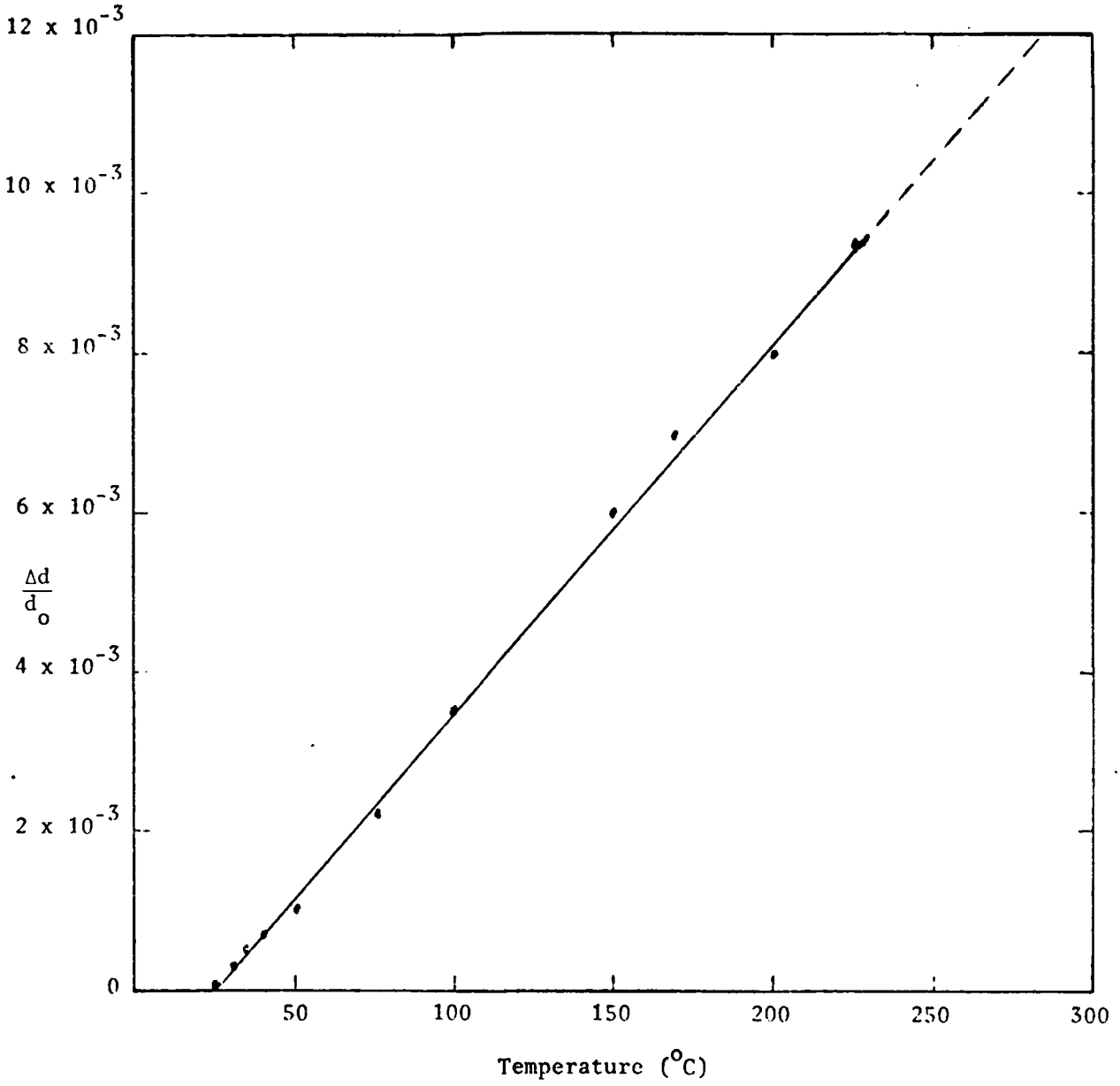

Figure 5

Static Thermal Expansion of the KAP Crystal Lattice Parameter d Over the Range 25° to 225°C

The straight line represents a constant expansion coefficient of 4.6×10^{-5}/K. These lattice spacing values were measured using crystal x-ray diffraction and a resistance wire heated thin piece of crystal.

quite reasonable to use the same expansion coefficient extrapolated over at least a substantial portion of the total range. The actual nonlinearity in the expansion curve, of course, need not be zero over such a large temperature range. Thus this expansion coefficient probably should be considered only a reasonable estimate for the higher expansion levels. Accordingly fairly large (but difficult to assess) errors must be attached to the inferred temperature rises quoted above, i.e., these temperature rises should still be best considered as qualitative results. Nevertheless, all indications are that KAP can be superheated to very high temperatures (even as much as 1000 K to 1500 K or more above the crystal melting point) without destruction of the Bragg reflection efficiency.

4.5 ESTIMATES OF ENERGY DEPOSITION AND DOSE LEVELS

The energy deposition and dose levels achieved in these experiments can only be estimated with the information now available. One estimate of these quantities can be derived from the expansion data themselves as follows. The standard estimate of heat capacity for such solids is given by $C_p = 3\ n\ R = 5.96\ n$ cal/K-mole where R is the universal gas constant and n is the number of atoms in a single molecule of the solid. The result for KAP, with n = 18 and one mole = 204 g, is $C_p = 107$ cal/K-mole, or 0.53 cal/g-K. This, together with the temperature rises suggested previously, would correspond to dose levels of ~ 500 to 1000 cal/g and perhaps even more. Such dose levels, for instance, would be produced by ~ 50 - 100 mJ/cm^2 of 0.3-keV radiation into the KAP, using the known x-ray absorption cross-sections. These levels are within the range to be expected from the limited knowledge of the x-ray source characteristics available. The data described in 3.3 show that ~ 10 mJ/sr of 1 keV and higher energy line radiation is produced by a low-energy 200-ps shot. At the 1-cm distance used in these experiments, the 10 mJ/sr results in a fluence of 10 mJ/cm^2. A comparable level should be produced by the longer but substantially more energetic shots used in these experiments. As noted earlier, the lower-energy radiation, however, is produced at a substantially greater level than this and hence would be in the general range suggested by the expansion data as noted above.

Section 5
TIME-DEPENDENT OBSERVATIONS ON CRYSTAL X-RAY DIFFRACTION

5.1 INTRODUCTION

Additional information on the nature of the effects produced by high dose-rate x-ray irradiation of crystal spectrometers beyond that obtained by the passive film recording would, of course, be very desirable. Accordingly a study of some time-dependent aspects of the phenomena has been carried out making use of a fast scintillator-streak-camera combination. These results, while they do not uniquely define the dynamics of the phenomena involved do establish certain characteristics which help clarify the potential limits to crystal spectrometer use and to define the nature of the crystal behavior under intense x-ray irradiation.

5.2 EXPERIMENTAL ARRANGEMENT AND TECHNIQUES FOR THE STREAK-CAMERA STUDIES

The overall experimental arrangement for the time-dependent experimental studies, exclusive of the laser system, is shown schematically in Fig. 6. (The laser system remained as shown in Fig. 1 for the time-integrated observations.) Briefly, as before for the time-integrated studies, the laser pulse was focused onto a target within a vacuum chamber and the resultant x rays were Bragg reflected from a crystal sample and directed onto a scintillator placed at one of the chamber observation ports. The x-ray produced scintillator light was optically relayed to a streak camera which was externally triggered in precise time relation with the light pulse. The trigger pulse for the streak camera was initiated by a portion of the laser beam which was split off just after leaving the oscillator and directed across the room to a trigger generator placed close to the streak camera. This experimental arrangement is discussed in more detail in the following paragraphs.

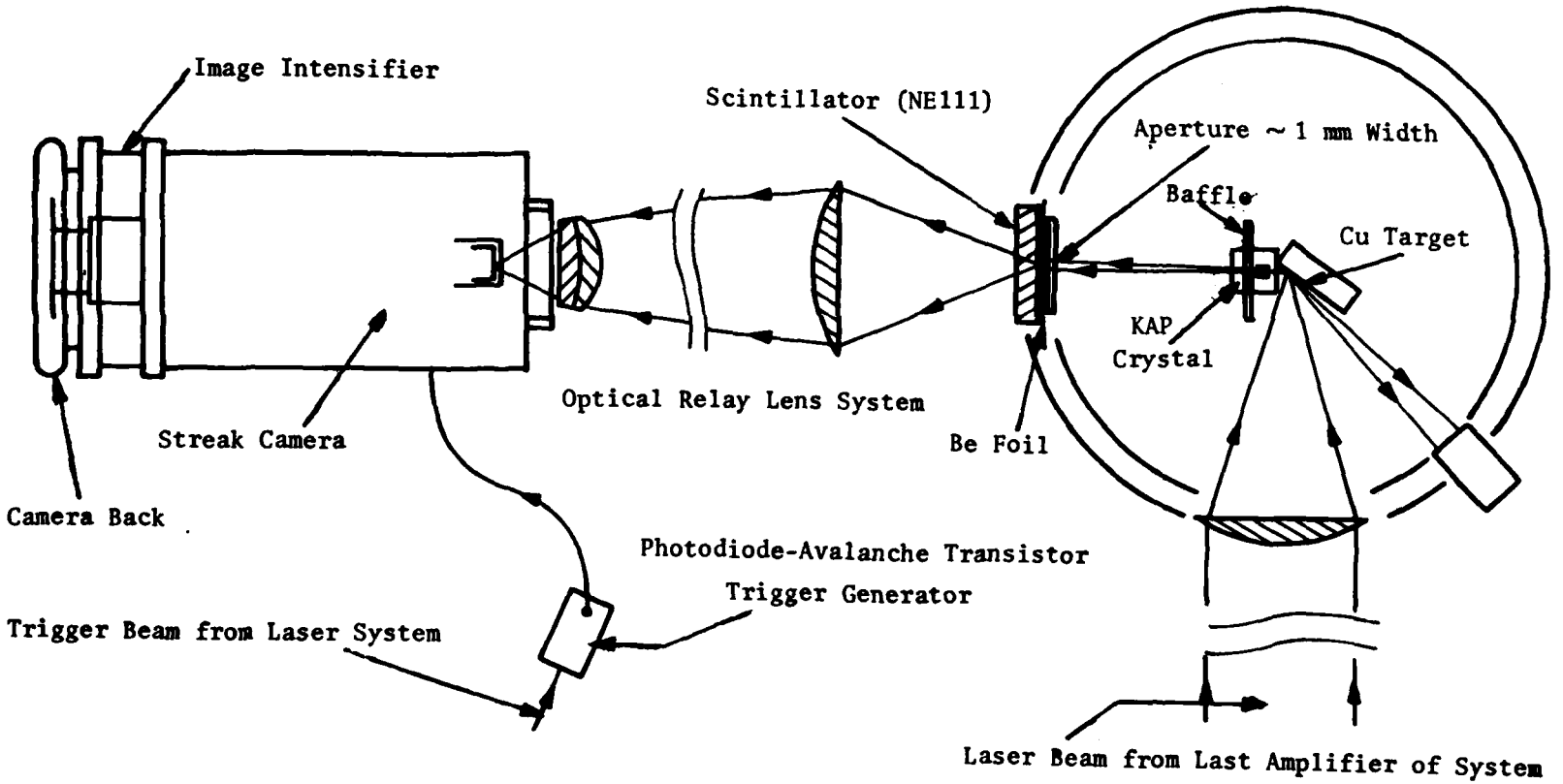

Figure 6

General Schematic of Experimental Arrangement (Horizontal Plan View)
for the Crystal Spectrometer Time-Dependent Investigations

The target chamber configuration has been changed from the earlier studies by the substitution of a Be-filtered Al-coated scintillator for the x-ray film pack. In addition, to achieve adequate scintillator luminosity, it was necessary to use thinner Be foils as well as to more tightly baffle the KAP crystal surface against the intense lower-energy but non-Bragg scattered x rays. The laser configuration is as already shown in Fig. 1.

The arrangement of the target chamber was the same as that shown in Fig. 2 for the time-integrated studies except that the film holder was replaced with a disc of NE111 scintillator 3.0-mm thick and 44 mm in diameter and which also functioned at the same time as the vacuum chamber window. In addition, it proved necessary to more tightly baffle the reflecting surface actually viewed by the streak camera because the intense lower energy x rays would otherwise produce too large a background via incoherent (non-Bragg) scattering. The scintillator, with both surfaces polished, had $\sim$ 170 nm of aluminum evaporated onto the x-ray entrance face. This helped provide the necessary light shield and in addition increased the light collection efficiency by about 90% (from a calculation using known optical constants for aluminum and the scintillation material). The scintillator light is produced with an exponential depth profile with a scale depth only $\sim$ .5 μm and thus the direct light and reflected light both appear to originate in a line source of very small total depth with no discernible effect produced on the resolution achieved by the streak camera. The scintillator also is covered with two pieces of 0.4-μm thick beryllium foil both for additional light shielding and to suppress the relatively low-energy x rays and extreme ultra violet. A vertical slit $\sim$ 1.4-mm wide and centered on the scintillator disc was used to create a narrow vertical spectral band whose image could then be swept in the direction normal to that of the energy dispersion. This scintillator assembly was mounted externally on the target chamber at a 90^{o} port with a 15.4-cm separation between the x-ray source and the scintillator front face.

The optical relay system was constructed of lenses already available in the laboratory and consisted of a collector which was a 78-mm effective diameter aspheric lens of focal length $\sim$ 109 mm--a duplicate of the target chamber laser beam focus lens, and a final achromatic lens of effective diameter 41 mm and focal length $\sim$ 45 mm. These focal lengths are approximate values for the light in the 380 - 390-nm wavelength range at which the scintillator has its output peak. The small diameter of the second lens resulted in a certain amount of vignetting, for instance, about 10 percent of the light is lost from the periphery of an object of

diameter 4 mm centered on the system optic axis. The preliminary focusing of the optical system was accomplished by illuminating a substitute target screen at the normal position of the scintillator entrance face. The illumination was that from an incandescant light but heavily filtered for the blue-violet by two Kodak Wratten Type 39 filters. Because of the system chromatic aberration (primarily because of the single element collector lens) even this procedure did not produce a sufficiently accurate focus and final adjustment was made by firing the laser and streak camera and adjusting the focus to produce the sharpest x-ray spectral line structure in the streak record.

The streak camera used in this work was a Hadland Photonics Limited, Imacon Model 675 with an S20 electrostatically-focused streak camera tube. The unit incorporated an image intensifier of $\sim 10^5$ maximum gain with a fiber optic output stage. The output was recorded in a camera which was arranged so that the film could be brought into direct contact with the fiber-optic output plate. Polaroid Type 410 film was used to record the streak data because of its high speed (Type 47 was inadequate even with the highest image intensifier gain). The streak speeds available with this unit range from 0.03 ns/mm to 10 ns/mm--for this work speeds of 0.5 -1.2 ns/mm were found to be appropriate. The time resolution obtained with this overall system is composed of three major parts--the 0.6 ns due to the NE111 scintillator effective pulse width and that due to the finite width of the slit on the scintillator which amounts to about 3 ns for the sweep speeds typically used and an intermediate contribution due to the chromatic aberration-induced image resolution loss. This could have been improved with faster sweeps but was judged adequate for the signal levels and time structure actually observed. A narrower slit would of course also have improved the effective time resolution, but the signal levels achieved precluded use of any very substantially narrower slit. The overall system magnification from the scintillator front face to the Polaroid film was about 4.

The streak camera was triggered by an externally generated electrical pulse which was in turn initiated by a pulse of laser light. A pellicle beam splitter was used to split off about 5% of the laser beam immediately after the pulse left the oscillator and first Pockels cell optical gate. This small laser pulse was then directed across the room to a trigger generator placed adjacent to the streak camera. The main laser beam then proceeded through the folded-path amplifier chain and thereby achieved sufficient optical delay relative to the trigger pulse that the internal trigger delays in the streak camera could be matched. The final timing adjustment was achieved by using direct x-ray illumination (non-Bragg reflected x rays) for greater signal level and ease of use. These latter adjustments were made by using varying lengths of cable between the trigger generator and the streak camera trigger input. The final arrangement then provided stable triggering with precise timing relationship to the laser-generated x-ray pulses such that the resultant streak always appeared at the same relative position on the film record for each successive shot.

5.3 EXPERIMENTAL RESULTS

Many streak records were obtained with the system as described above in which various parameters were adjusted to achieve optimum signals. In particular, various filter and baffle arrangements were tested to try to improve the signal level and signal-to-noise ratio. The final choice was a Be filter of 0.8-μm total thickness together with a relatively tight baffle arrangement. A sweep speed of 0.8 ns/mm was used together with an x-ray pulse duration of 10 ns (6-ns duration pulses had been used in all the preliminary work), however, the longer pulses were expected to be more informative and were used with the finalized arrangement. The laser pulse energy for these observations was typically in the 4-6-J range, rather lower than originally hoped for because it proved impossible to reach the same laser system performance level that had been achieved earlier for the time-integrated studies. With these experimental parameters, the typical streak records which resulted are shown in Figs. 7 and 8, together with representative oscilloscope traces of the x-ray yield in this same

Figure 7

Streak Camera Records for Cu X-Ray Lines Diffracted by KAP (Set I)

The streak photographs, b, are of two typical moderate intensity x-ray shots of duration 10 ns. The line in the center of the streak is at 1.09 keV energy. Time advances to the right and x-ray energy increases downward in these photographs. Typical XRD monitor oscilloscope traces of the x-ray intensity are shown above in a. Note that streak intensity does not fall off drastically indicating that Bragg reflection efficiency remains high throughout the pulse.

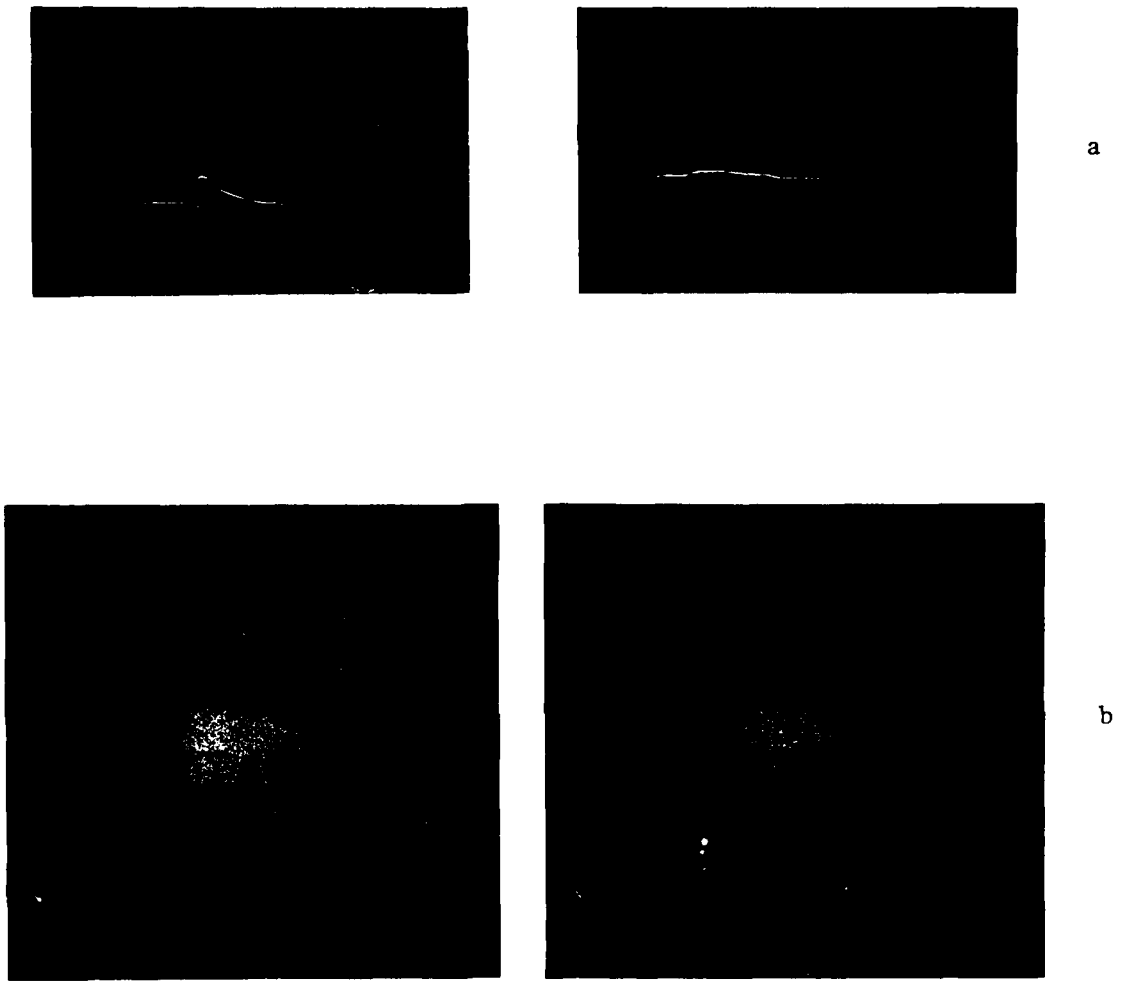

Figure 8

Streak Camera Records for Cu X-Ray Lines Diffracted by KAP (Set II)

Streak camera records, b, for different x-ray pulse shapes as shown in the corresponding XRD monitor oscilloscope traces, a. The conditions are otherwise as for Figure 7. As before, both the streak and the x-ray pulse have a duration of about 10 ns showing that the reflection is not destroyed, at least within the 10-ns time scale.

energy range as recorded by an XRD. The major line seen in the streaks results from the 1.093-keV copper x-ray line which was used instead of the 980-eV doublet because under the actual experimental conditions it could be produced with greater intensity. The doublet would have been otherwise preferable, both because of its lower energy (a better match to the heating profile) and because it is much more isolated in the spectrum. These streaks show little, if any, tendency to exhibit a slope, suggesting that the phenomena is in nearly steady-state equilibrium throughout most of the 10-ns pulse duration. A possibility that an accumulative change is taking place throughout the pulse duration is suggested in the observation that the line intensity in the streak has a tendency to remain relatively high, while the x-ray intensity, as monitored by the XRD, is dropping off rather drastically. This might indicate that progressive expansion of the crystal is occurring with a resultant increase in total reflection efficiency because of the resultant line broadening. The net result of the streak-camera observations is that the total reflection efficiency for a line remains high through the duration of a 10-ns pulse and perhaps even increases with time. Time-integrated film records of the line structure for typical shots in this sequence show that, while these shots have not produced as great a line distortion as was produced when the time-integrated studies were being carried out, a large portion of the reflected line intensity is occurring from strongly-heated material. Thus significant Bragg reflection must be taking place from heated material for times of the order of 10 ns. Whether or not an individual element of heated material Bragg reflects over this time scale cannot be determined from this data. Better x-ray line resolution in the streak camera and perhaps more intense x-ray pulses over a greater range of time scales including substantially shorter time scales might be required to give a definitive answer to this question.

Section 6
CONCLUSIONS AND RECOMMENDATIONS

A laboratory study of the effects of high dose-rate x-ray irradiation on the Bragg reflection of a KAP crystal has been carried out. It has been demonstrated that this crystal can be irradiated to a dose level with a resultant heating that produces a linear expansion of as much as several percent without destroying the Bragg reflection efficiency. The Bragg-reflected spectral lines then exhibit a corresponding distortion in which they show a sharp edge at the high-angle (or low-energy) side of the line and an extensive broadening on the low-angle (or high-energy) side of the line. Depending on the requirements of particular field measurements, this loss of effective resolution could severely limit the crystal usefulness in environments where high x-ray dose rates will result. Thus, if good resolution is desired in a future field measurement using KAP, the surface dose level should be limited to less than a few hundred cal/g. The expected dose levels and dose rates are of course easily constructed for a given experiment from the predicted spectrum and known absorption cross-sections in KAP. The time dependence of these phenomena was also investigated and it was found that the total reflection efficiency remains high throughout at least the 10-ns duration of the x-ray pulses used. There is, in fact, some suggestion that the reflection efficiency can progressively increase throughout the pulse irradiation. This effect might be expected because of the variation in lattice spacing over the x-ray penetration depth resulting from the heating profile vs. depth actually achieved in these irradiations. Again, depending on the requirements of a particular measurement, such variations with time of total Bragg reflection efficiency could be unacceptable even when high resolution was not a requirement. The restriction on the dose levels that can be used for field experiments is probably even more severe from this effect than for the loss of resolution. It is however, impossible at the present time, to suggest a practical dose limit other than that it should undoubtedly be even lower than the above limit.

Several improvements and extensions of these experimental studies can be recommended. First it should be remembered that the very high heating levels achieved in these studies resulted from the use of quite low x-ray energies (sub-keV) and correspondingly only a very thin crystal layer was heated. It would be desirable to carry out these experiments with greater x-ray power available so that e.g., the copper x rays of energy 1 keV and above could be used to provide the crystal heating. Then e.g., the 980-eV copper doublet x rays would penetrate only into strongly-heated material and the resulting phenomena might well exhibit different characteristics, especially in the streak-camera studies. These results would undoubtedly then have even a more direct relevance to typical field measurements. In addition, the energy deposition and dose levels developed with the keV radiation could be much more accurately determined than for the present sub-keV x-ray irradiation. It should be pointed out that this greater power will be available when the laser upgrading currently in the planning stages has been completed. Secondly, a survey of the behavior of other crystals of interest in field measurements would be desirable. It might be e.g., that high melting-point inorganic crystals would exhibit substantial differences from those observed with the low melting point KAP organic crystal. In addition, several improvements in the instrumentation and techniques used in these studies should be undertaken for any such additional work. Improved resolution in the passive x-ray spectrometer studies would be possible when greater x-ray power is available since the separation of the film from the x-ray source can then be substantially increased. Similarly, improved resolution in the time-dependent studies should result from this change. In addition, the optical relay system resolution could be improved still further by achieving a fully-achromatic system. Finally, it would undoubtedly be very useful to have a theoretical study of these phenomena undertaken in order to develop a more complete and more quantitative understanding. This in turn would then make it possible to achieve the more reliable extrapolations necessary to adequately design the experiments to be used under actual field conditions.

DISTRIBUTION LIST

DEPARTMENT OF DEFENSE

Defense Technical Information Center
12 cy ATTN: DD

Defense Nuclear Agency
ATTN: DDST
ATTN: SPTD, T. Kennedy
ATTN: SPTD, R. Webb
ATTN: SPTD, W. Summa
ATTN: STRA
4 cy ATTN: TITL

Field Command
Defense Nuclear Agency
ATTN: FCTMD
ATTN: FCPR
ATTN: FCTMEI
2 cy ATTN: FCTMOF

Field Command
Defense Nuclear Agency
Livermore Division
ATTN: FCPRL

Assistant to the Secretary of Defense
Atomic Energy
ATTN: Executive Assistant

Undersecretary of Def. for Rsch. & Engrg.
ATTN: Strategic & Space Systems (OS)

DEPARTMENT OF THE ARMY

BMD Advanced Technology Center
Department of the Army
ATTN: ATC-T, M. Capps

Electronics Tech. & Devices Lab.
U.S. Army Electronics R&D Command
ATTN: DELET-R, S. Kronenberg

Harry Diamond Laboratories
Department of the Army
ATTN: DELHD-I-TL
ATTN: DELHD-N-P, F. Wimenitz

U.S. Army Missile R&D Command
ATTN: Redstone Scientific Info. Ctr.

U.S. Army Nuclear & Chemical Agency
ATTN: Library

DEPARTMENT OF THE NAVY

Naval Postgraduate School
ATTN: Code 0142

Naval Research Laboratory
ATTN: Code 2627

Naval Surface Weapons Center
ATTN: Code F31

DEPARTMENT OF THE AIR FORCE

Air Force Weapons Laboratory
ATTN: SUL

Deputy Chief of Staff
Research, Development, & Acq.
Department of the Air Force
ATTN: AFRDQSM

DEPARTMENT OF ENERGY CONTRACTORS

Lawrence Livermore Laboratory
ATTN: Document Control for L-200, J. Cortez
ATTN: Document Control for B. Hudson
ATTN: Document Control for L-24, D. Vik
ATTN: Document Control for L-14, W. Dickinson
ATTN: Document Control for L-38, H. Reynolds
ATTN: Document Control for L-203, L. Germain
ATTN: Document Control for Technical Information Dept. Library
ATTN: Document Control for L-21, D. Oakley

Los Alamos Scientific Laboratory
ATTN: Document Control for P. Lyons
ATTN: Document Control for R. Thorn
ATTN: Document Control for H. Agnew
ATTN: Document Control for R. Brownlee
ATTN: Document Control for P. Whalen
ATTN: Document Control for C. Keller
ATTN: Document Control for MS 364

Sandia Laboratories
ATTN: Document Control for 3141
ATTN: Document Control for B. Benjamin
ATTN: Document Control for J. Plimpton
ATTN: Document Control for J. Walker
ATTN: Document Control for C. Broyles

DEPARTMENT OF DEFENSE CONTRACTORS

EG&G, Inc.
ATTN: M. Nelson

General Electric Company—TEMPO
ATTN: DASIAC

Institute for Defense Analyses
ATTN: Classified Library

JAYCOR
ATTN: L. Scott

Kaman Sciences Corp.
ATTN: F. Shelton

Lockheed Missiles and Space Co., Inc.
ATTN: D. Kohler
ATTN: S. Salisbury
ATTN: J. Pronko
ATTN: T. Fisher
ATTN: R. Bardin
ATTN: R. Smith
2 cy ATTN: L. Chase

DEPARTMENT OF DEFENSE CONTRACTORS (Continued)

R & D Associates
ATTN: R. Poll
ATTN: C. MacDonald
2 cy ATTN: Technical Information Center

DEPARTMENT OF DEFENSE CONTRACTORS (Continued)

Science Applications, Inc.
ATTN: R. Miller

Systems, Science & Software, Inc.
ATTN: C. Dismukes